Electronic Supplementary Information (ESI)

Framework-to-Carbon Conversion Strategy for Nitrogen–Silicon co-Doped Microporous Carbons with Superior Energy Storage Performance

Zhe Wei Zhang,[1] Yousra M. Nabil,[1] Ahmed E. Hassan,[2] and Ahmed F. M. EL-Mahdy*[1]

[1] Department of Materials and Optoelectronic Science, National Sun Yat-Sen University,
Kaohsiung 80424, Taiwan.

[2] Interdisciplinary Research Center for Hydrogen Technologies and Carbon Management (IRC-HTCM), King Fahd University of Petroleum & Minerals, Dhahran 31261, Saudi Arabia

*To whom correspondence should be addressed

E-mail: ahmedelmahdy@mail.nsysu.edu.tw

S1. Materials

All solvents and reagents were obtained from commercial suppliers and used as received unless otherwise noted. 4-Bromobenzaldehyde dimethyl acetal, *n*-butyllithium (n-BuLi, 2.5 M in hexane), silicon tetrachloride (SiCl4), benzene-1,4-dicarbonitrile, tert-butoxide potassium (t-BuOK), dimethyl sulfoxide (DMSO, anhydrous), tetrahydrofuran (THF, anhydrous), hydrochloric acid (HCl solutions), sodium bicarbonate ($NaHCO_3$), ethyl acetate, methanol (MeOH), and deionized (DI) water were purchased from Sigma-Aldrich and used without further purification. Lithium bis(trimethylsilyl)amide ($LiN(SiMe_3)_2$) at a concentration of 1.0 M in THF was obtained from Sigma-Aldrich. All reactions were performed under a nitrogen atmosphere using standard Schlenk or sealed-tube techniques. The precursors Si-4CHO, TP-$2NHNH_2$, and BP-$2NHNH_2$ were synthesized following the procedures described in the experimental section.

S2. Characterizations

Fourier-transform infrared spectroscopy (FTIR) was performed using a Bruker Tensor 27 FTIR spectrophotometer and the standard KBr pellet method, collecting 32 scans at a resolution of 4 cm^{-1}. Solid-state nuclear magnetic resonance (SSNMR) spectra were recorded on a Bruker Avance 400 MHz NMR spectrometer equipped with a magic-angle spinning (MAS) probe, with 32,000 scans collected per sample. Thermogravimetric analysis (TGA) was conducted using a TA Instruments Q-50 analyzer under a nitrogen flow (50 mL min^{-1}) from 40 to 800 °C at a heating rate of 20 °C min^{-1} in a platinum crucible. Nitrogen adsorption–desorption isotherms were obtained on a BelSorp Max analyzer at 77 K. Prior to measurements, samples (50 mg) were Soxhlet-extracted with anhydrous THF for 24 h, followed by vacuum activation at 150 °C for 10 h. The specific surface area was determined using the Brunauer–Emmett–Teller (BET) method, and pore size distributions were derived using quenched solid-state density functional theory (QSDFT). Scanning electron microscopy (SEM) images were captured using a JEOL JSM-7610F field emission scanning electron microscope. Samples were sputter-coated with a thin platinum layer for 100 s before imaging. Transmission electron microscopy (TEM) was carried out on a JEOL JEM-2100 microscope operating at 200 kV to analyze the internal morphology and pore structure. Powder X-ray diffraction (XRD) patterns were recorded on a Bruker D8 Advance diffractometer equipped with Cu Kα radiation (λ = 1.5406 Å), operating at 40 kV and 40 mA, with a scanning rate of 2° min^{-1} over a 2θ range of 5–80°. Raman spectra were obtained using a Horiba LabRAM HR Evolution spectrometer with

a 532 nm laser excitation source, allowing evaluation of the graphitic structure and defect density of the carbon materials. X-ray photoelectron spectroscopy (XPS) measurements were performed on a Thermo Scientific ESCALAB 250Xi spectrometer equipped with a monochromatic Al Kα (1486.6 eV) X-ray source. The binding energy scale was calibrated using the C 1s peak at 284.8 eV as a reference. Deconvolution of the C 1s, N 1s, and Si 2p spectra was conducted using CasaXPS software to determine the chemical bonding environments and elemental compositions of the samples.

S3. Synthetic Procedures

Synthesis of tetrakis(4-formylphenyl)silane (Si-4CHO)

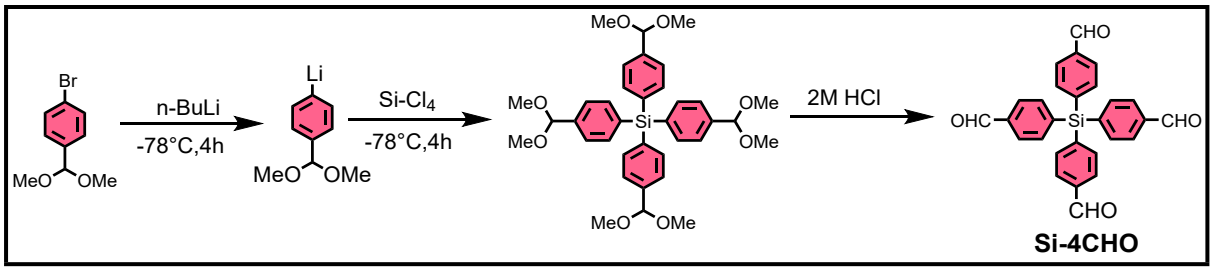

Scheme S1. Synthesis of Si-4CHO.

4-Bromobenzaldehyde dimethyl acetal (3.01 g, 13.0 mmol) was dissolved in anhydrous tetrahydrofuran (THF, 100 mL) under a nitrogen atmosphere. A solution of *n*-butyllithium (*n*-BuLi, 2.5 M in hexane, 10.4 mL, 26 mmol) was added dropwise at –78 °C over 45 min. The reaction mixture was stirred for 4 h at –78 °C, followed by the slow addition of silicon tetrachloride ($SiCl_4$, 0.57 mL, 5 mmol). The mixture was further stirred for 4 h at –78 °C and then allowed to warm to room temperature, stirring overnight. The reaction was quenched with 2 M HCl (40 mL) and extracted with ethyl acetate (3 × 50 mL). The combined organic layers were washed with brine, dried over anhydrous Na_2SO_4, and concentrated under reduced pressure to yield a light-yellow solid, identified as $Si(4\text{-}C_6H_4CH(OCH_3)_2)_4$, which was directly hydrolyzed without purification.

The crude product was dissolved in a 1:1 (v/v) mixture of THF (60 mL) and 2 M HCl and refluxed overnight. After cooling to room temperature, the reaction mixture was poured into a saturated $NaHCO_3$ solution (50 mL) and extracted with ethyl acetate (3 × 50 mL). The combined organic layers were washed with brine, dried over Na_2SO_4, filtered, and concentrated under reduced pressure to afford Si-4CHO as an off-white solid.

Synthesis of 1,4-benzenedicarboximidamide ($TP\text{-}2NHNH_2$)

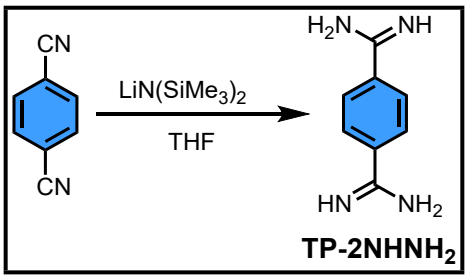

Scheme S2. Synthesis of $TP\text{-}2NHNH_2$.

To a stirred solution of benzene-1,4-dicarbonitrile (1.24 g, 9.7 mmol) in anhydrous tetrahydrofuran (THF, 30 mL) was added a solution of lithium bis(trimethylsilyl)amide ($LiN(SiMe_3)_2$, 1 M in THF, 40 mL) dropwise at 0 °C over 30 min under a nitrogen atmosphere. The reaction mixture was then allowed to warm to room temperature and stirred for 3 h, after which it was cooled again to 0 °C. The reaction was quenched by carefully adding 6 M HCl in ethanol (40 mL) and stirred for an additional 2 h. The resulting precipitate was filtered, washed thoroughly with diethyl ether, and recrystallized from a water–ethanol mixture to afford terephthalamidinium dichloride ($TP\text{-}2NHNH_2$) as an off-white solid.

Synthesis of and [1,1'-biphenyl]-4,4'-bis(carboximidamide) ($BP\text{-}2NHNH_2$)

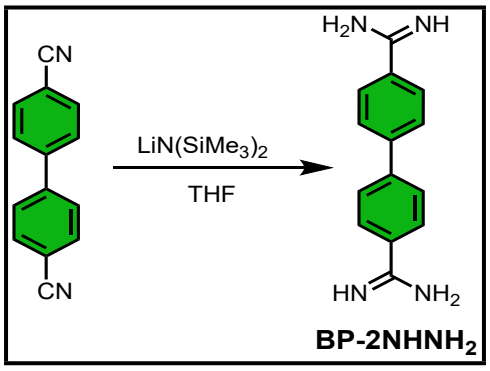

Scheme S3. Synthesis of $BP\text{-}2NHNH_2$.

To a stirred solution of [1,1'-biphenyl]-4,4'-dicarbonitrile (1.98 g, 9.7 mmol) in anhydrous tetrahydrofuran (THF, 50 mL) was added a solution of lithium bis(trimethylsilyl)amide ($LiN(SiMe_3)_2$, 1 M in THF, 40 mL) dropwise at 0 °C over 30 min under a nitrogen atmosphere. The reaction mixture was then allowed to warm to room temperature and stirred for 3 h, after which it was cooled again to 0 °C. The reaction was quenched by carefully adding 6 M HCl in ethanol (60 mL) and stirred for an additional 2 h. The resulting precipitate was filtered, washed

thoroughly with diethyl ether, and recrystallized from a water–ethanol mixture to afford terephthalamidinium dichloride (BP-2NHNH$_2$) as an off-white solid.

Synthesis of Si-CTF-1

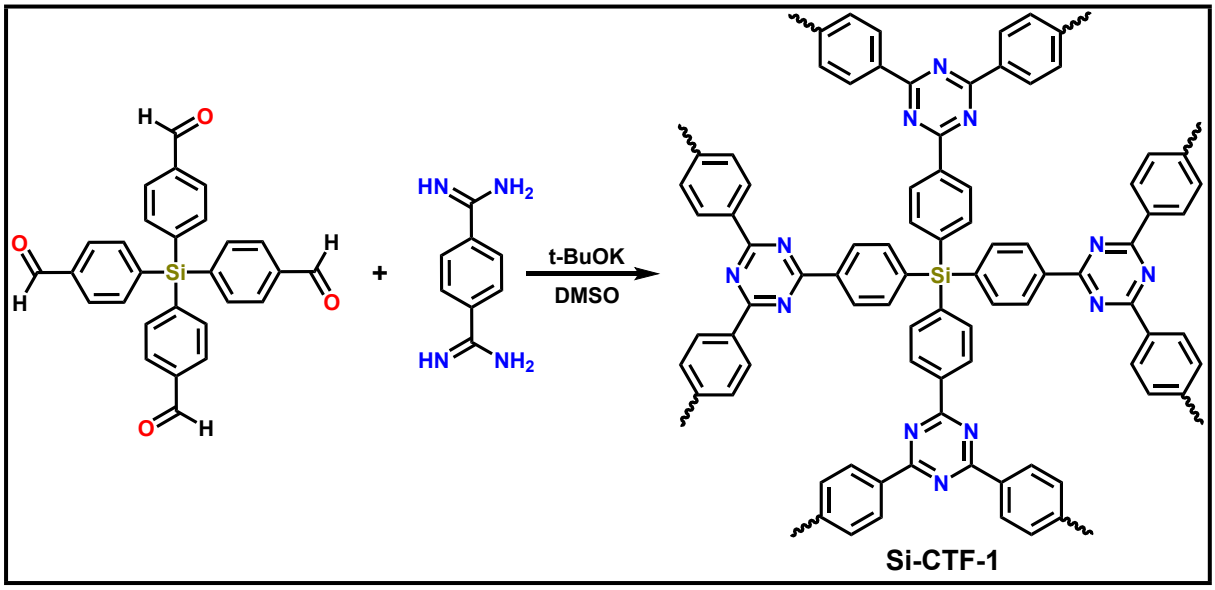

Scheme S4. Synthesis of Si-CTF-1.

Si-4CHO (100 mg, 0.223 mmol) and TP-2NHNH$_2$ (210 mg, 0.892 mmol) were dissolved in anhydrous dimethyl sulfoxide (DMSO, 10 mL). *tert*-Butoxide potassium (t-BuOK, 200 mg, 1.782 mmol) was added as a base catalyst. The reaction mixture was transferred to a thick-walled glass tube, which was evacuated through three freeze–pump–thaw cycles to remove dissolved gases and then flame-sealed under vacuum. The sealed tube was gradually heated to 100 °C and maintained for 24 h, followed by stepwise heating to 120 °C for 24 h and 160 °C for 48 h. After cooling to room temperature, the resulting solid was collected by centrifugation and washed sequentially with methanol, 1 M HCl, and deionized water (2 × each, 2 min per wash). The obtained solid was filtered and dried in an oven at 70 °C overnight, yielding the Si-CTF-1 powder as the final product.

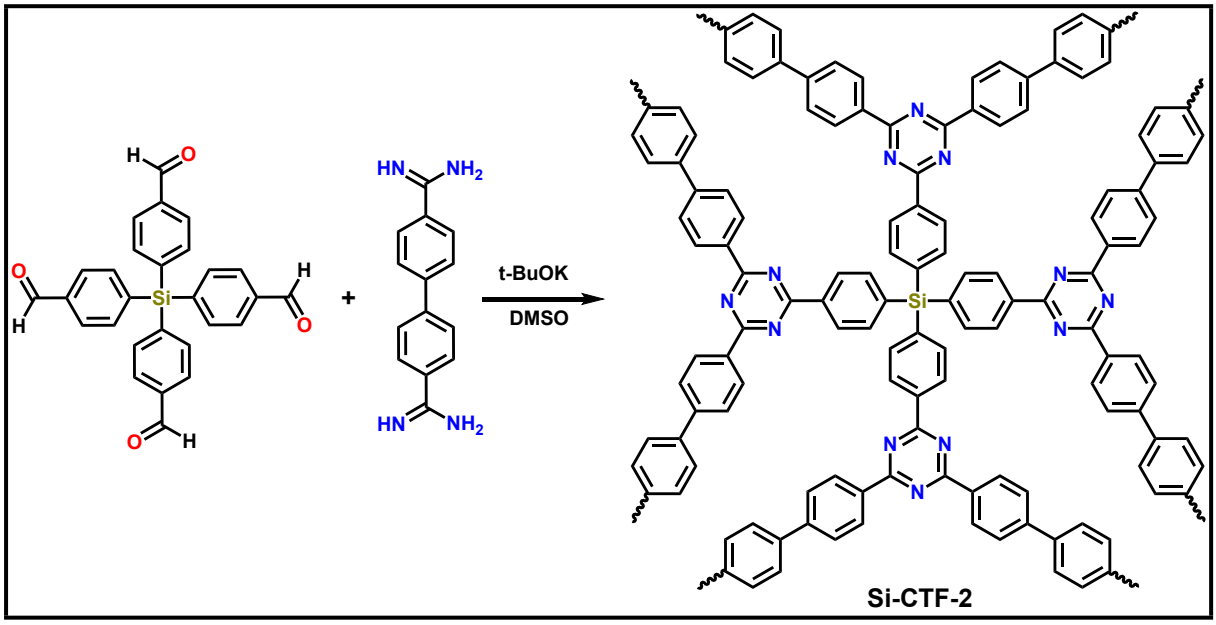

Scheme S5. Synthesis of Si-CTF-2.

Si-4CHO (100 mg, 0.223 mmol) and BP-2NHNH$_2$ (278 mg, 0.892 mmol) were dissolved in anhydrous dimethyl sulfoxide (DMSO, 10 mL). *tert*-Butoxide potassium (t-BuOK, 200 mg, 1.782 mmol) was added as a base catalyst. The reaction mixture was transferred to a thick-walled glass tube, which was evacuated through three freeze–pump–thaw cycles to remove dissolved gases and then flame-sealed under vacuum. The sealed tube was gradually heated to 100 °C and maintained for 24 h, followed by stepwise heating to 120 °C for 24 h and 160 °C for 48 h. After cooling to room temperature, the resulting solid was collected by centrifugation and washed sequentially with methanol, 1 M HCl, and deionized water (2 × each, 2 min per wash). The obtained solid was filtered and dried in an oven at 70 °C overnight, yielding the Si-CTF-2 powder as the final product.

S4. FTIR and NMR Spectral Profiles of Monomers

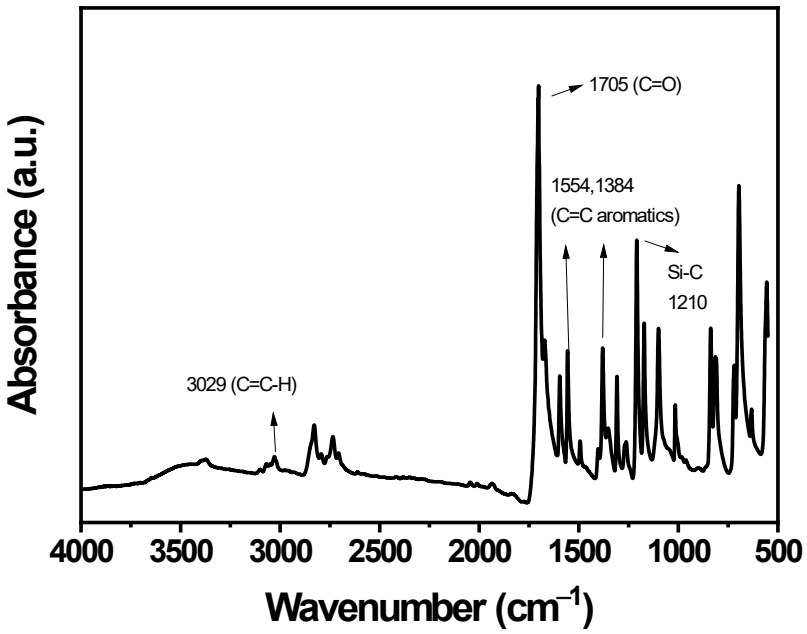

Figure S1. FT-IR spectrum of Si-CHO

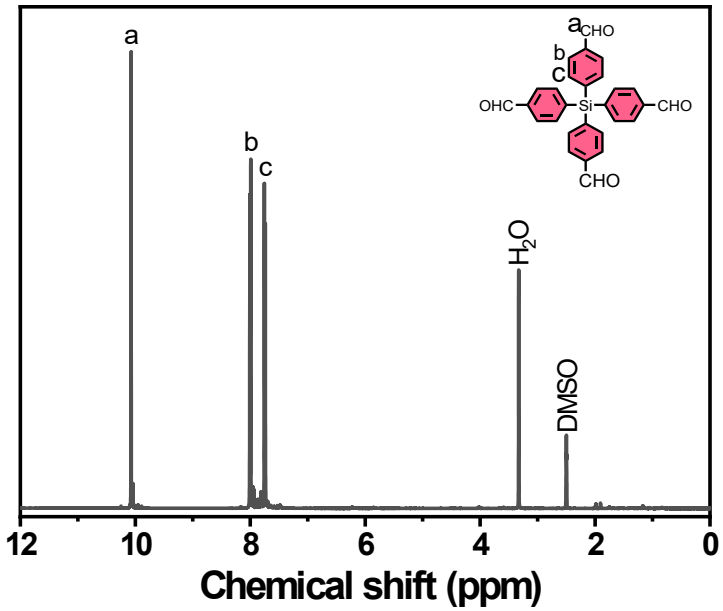

Figure S2. ^{1}H NMR spectrum of Si-4CHO.

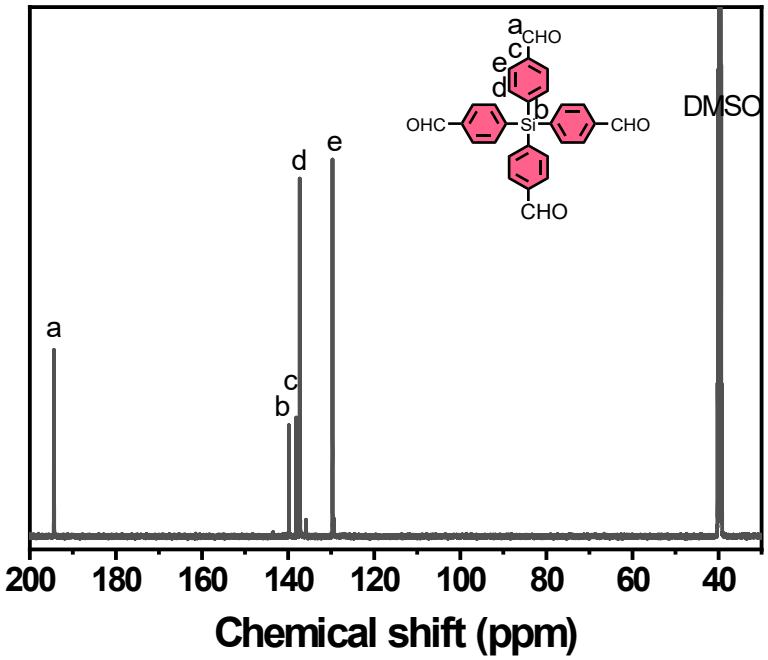

Figure S3. ^{13}C NMR spectrum of Si-4CHO.

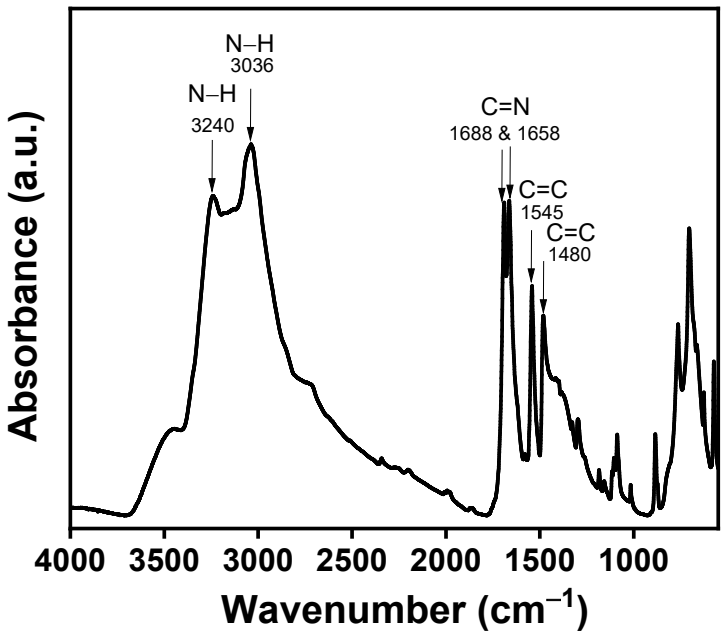

Figure S4. FT-IR spectrum of TP-2NHNH$_2$.

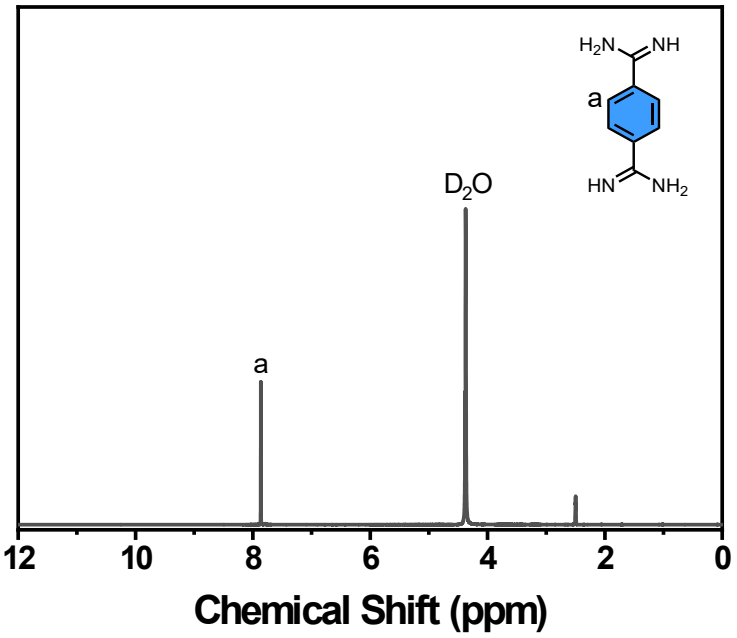

Figure S5. ^{1}H NMR spectrum of TP-2NHNH$_2$.

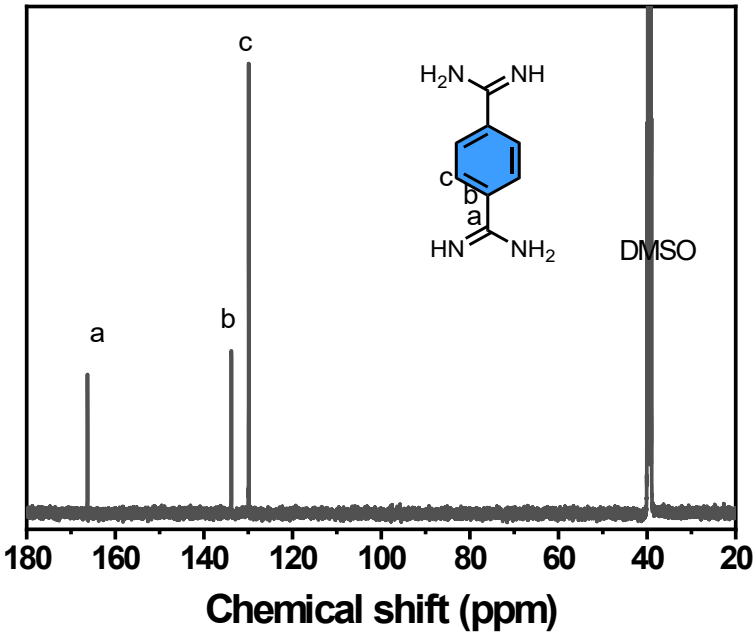

Figure S6. ^{13}C NMR spectrum of TP-2NHNH$_2$.

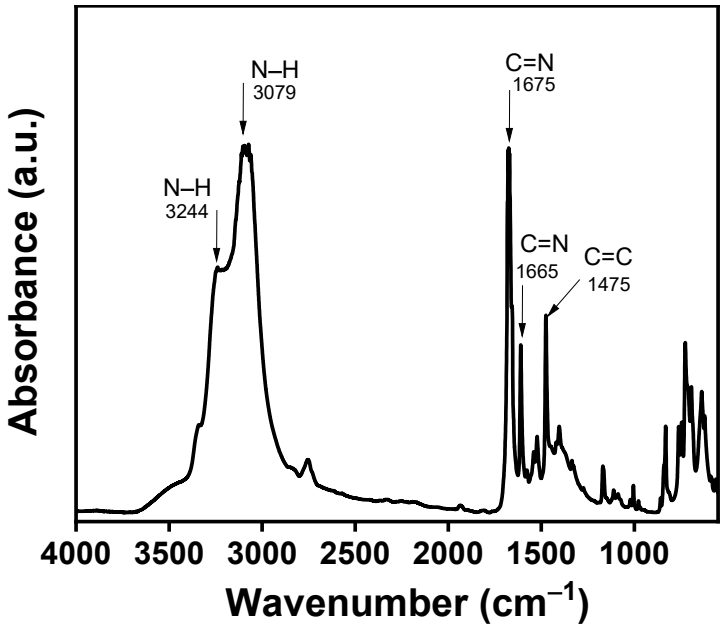

Figure S7. FT-IR spectrum of BP-2NHNH$_2$.

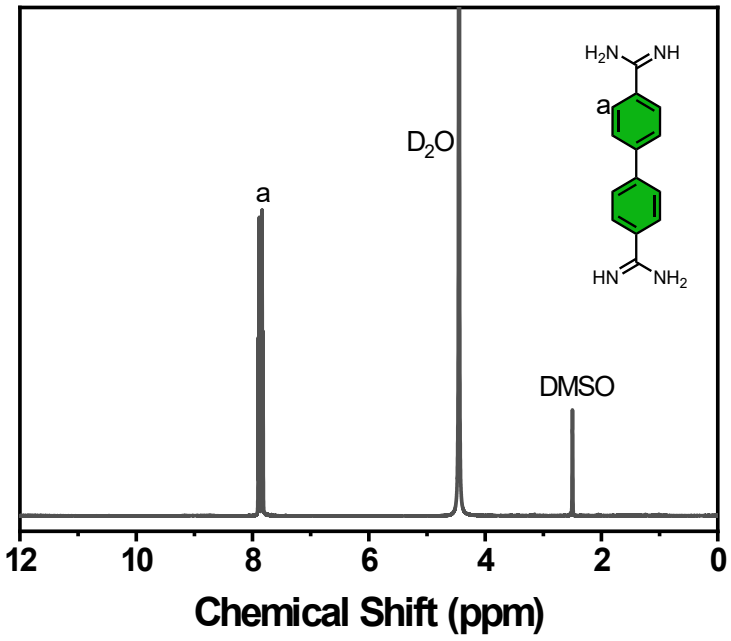

Figure S8. ^{1}H NMR spectrum of BP-2NHNH$_2$.

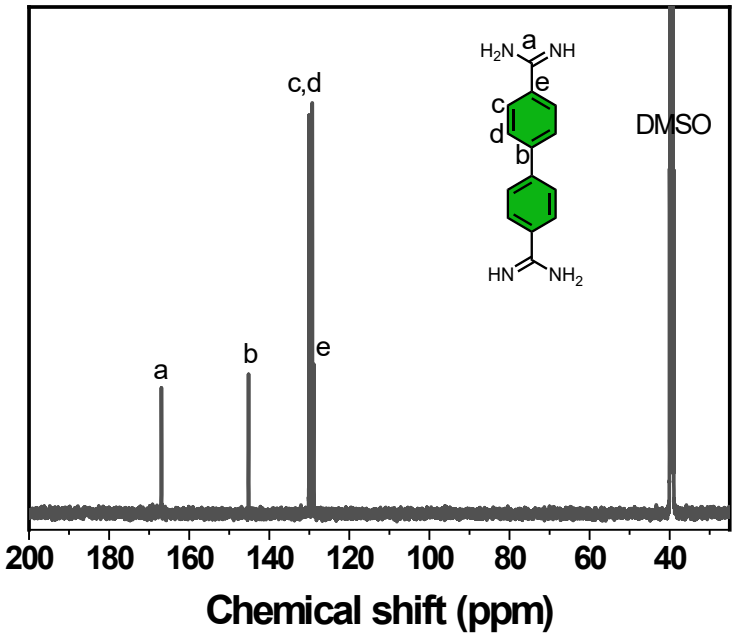

Figure S9. ^{13}C NMR spectrum of BP-2NHNH$_2$.

S5. Thermal Gravimetric Analysis of Si-CTFs

CTFs	T_{d10} (°C)	Char yield (%)
Si-CTF-1	396.86	53.77
Si-CTF-2	592.17	63.86

Table S1. Values of T_{d10}%, and Char yield of Si-CTF-1 and Si-CTF-2

S6. Surface Area Parameters

NSi@Cs	S_{BET} ($m^2 g^{-1}$)	Pore size (nm)	Pore Volume ($cm^3 g^{-1}$)
NSi@C-1	544	0.73	0.2185
NSi@C-2	732	0.99, 1.78	0.5921

Table S2. BET parameters of SiN@C-1 and SiN@C-2

S7. SEM and EDS imaging of the NSi@Cs

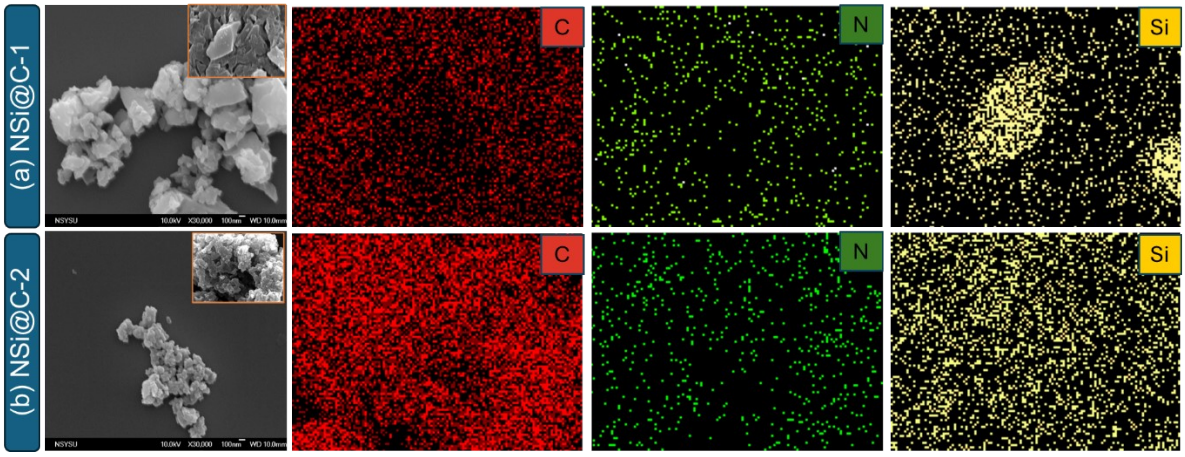

Figure S10. (a) SEM image of NSi@C-1 and the corresponding EDS element analysis of C, N, and Si elements. (b) SEM image of NSi@C-2 and the corresponding EDS element analysis of C, N, and Si elements.

S8. Raman data of the NSi@Cs

Table S3. I_D/I_G ratio of SiN@C-1 and SiN@C-2

NSi@Cs	I_D/I_G
NSi@C-1	1.08
NSi@C-2	1.04

S9. Thermal Gravimetric Analysis of the NSi@Cs

NSi@Cs	T_{d5} (°C)	Char yield (%)
NSi@C-1	743	90.5
NSi@C-2	752	91.0

Table S4. Values of T_{d5}%, and Char yield of NSi@C-1 and NSi@C-2

S10. X-ray Photoelectron Spectroscopy Analysis of the NSi@Cs

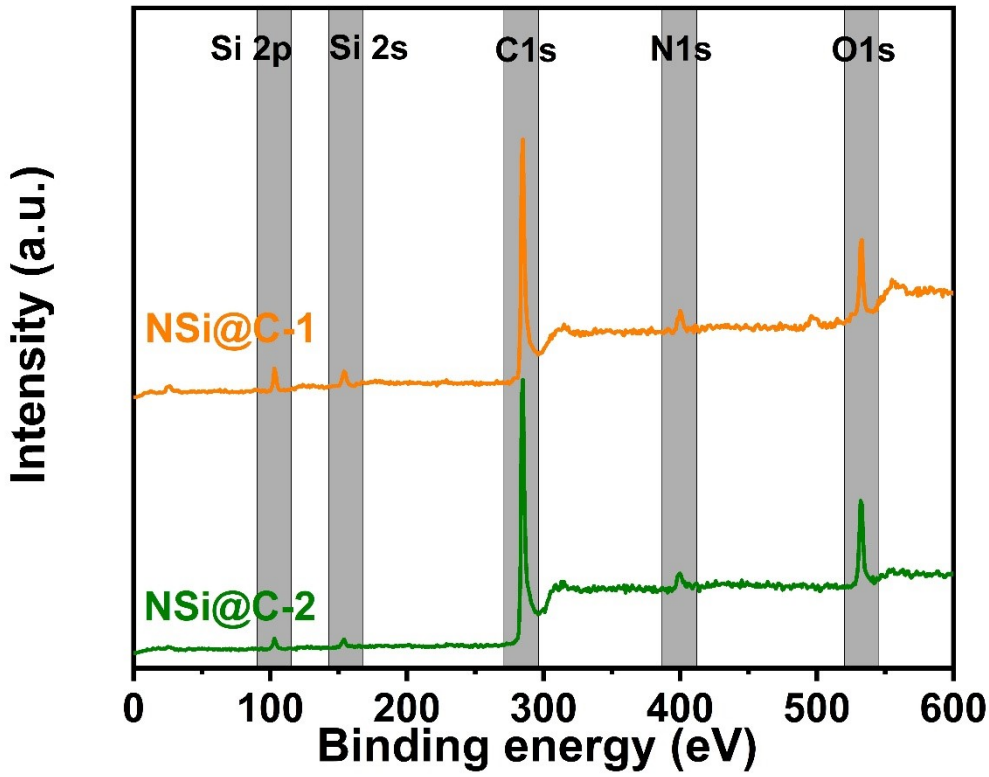

Figure S11. XPS survey spectra of NSi@C-1 and NSi@C-2.

Table S5. XPS fitting positions of NSi@C-1 and NSi@C-2

NSi@Cs	C species				N species				Si species	
	C=C	C–Si	C=N	C=O	*N*-Pyridine	*N*-Pyrrole	*N*-quaternary	*N*-Ozidized	Si–C	Si–O
NSi@C-1	285.2	285.6	287.0	289.1	399.3	400.4	401.4	403.2	102.6	104.2
NSi@C-2	285.4	286.1	287.3	289.0	398.8	400.2	401.7	403.0	103.7	105.2

Table S6. XPS fitting area fractions of NSi@C-1 and NSi@C-2

NSi@Cs	C species				N species				Si species	
	C=C	C–Si	C=N	C=O	*N*-Pyridine	*N*-Pyrrole	*N*-quaternary	*N*-Ozidized	Si–C	Si–O
NSi@C-1	63.42	11.23	12.35	13.00	34.40	36.80	21.70	7.10	93.37	6.63
NSi@C-2	71.95	10.59	9.26	8.18	35.90	42.30	13.80	8.0	92.26	7.74

S11. Electrochemical Assessment

Electrochemical measurements were conducted using a Zahner potentiostat in a standard three-electrode setup with 1 M KOH aqueous electrolyte. A glassy carbon electrode (GCE, diameter = 5.61 mm; area = 0.2475 cm^2) served as the working electrode, a platinum wire was used as the counter electrode, and a Hg/HgO electrode (RE-61AP, BAS) acted as the reference electrode. All reported potentials are referenced to Hg/HgO. The GCE surface was modified with conjugated polymer slurries prepared with slight modifications to previously reported procedures.[1-4] Each slurry contained 70 wt% conjugated polymer, 20 wt% carbon black, and 10 wt% Nafion dispersed in a solvent mixture of 0.2 mL ethanol and 0.8 mL deionized water, followed by sonication for 1 h. A 5 µL aliquot of the slurry was drop-cast onto the GCE surface and air-dried for 30 min before measurement.

Cyclic voltammetry (CV) was performed at scan rates ranging from 5 to 200 mV s^{-1}, and galvanostatic charge–discharge (GCD) tests were carried out within a potential window of −1.0 to 0 V (vs Hg/HgO) in 1 M KOH at current densities from 0.5 to 20 A g^{-1}. The specific capacitance (C_s) was derived from the GCD profiles using the following equation:[4,5]

$$Cs = (I\Delta t)/(m\Delta V) \qquad \text{(S1)}$$

Cs (F g^{-1}) represents the specific capacitance of the supercapacitor, where I (A) is the discharge current, ΔV (V) denotes the potential window, Δt (s) is the discharge time, and m (g) corresponds to the mass of the carbon deposited on the electrode. The energy density (E, Wh kg^{-1}) and power density (P, W kg^{-1}) were calculated according to equations (S2) and (S3), respectively:[5,6]

$$E = \frac{1000 \times C_s \times (\Delta V)^2}{2 \times 3600} \qquad \text{(S2)}$$

$$P = \frac{E}{(t/3600)} \qquad \text{(S3)}$$

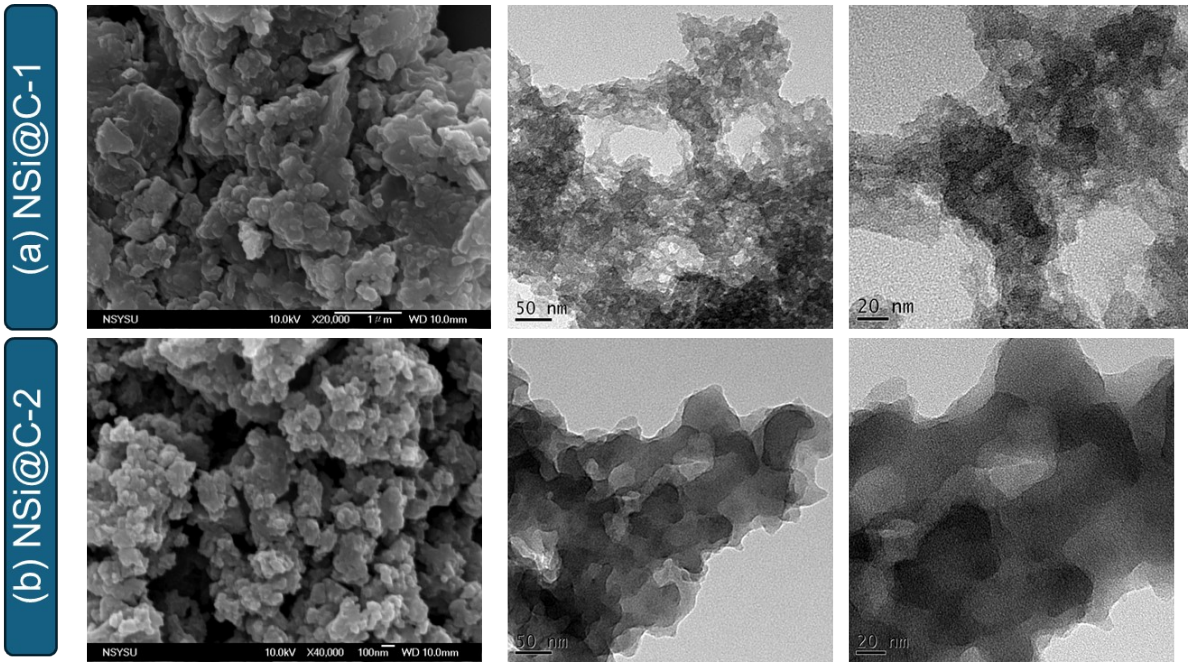

Figure S12. SEM and TEM images of (a) NSi@C-1 and (b) NSi@C-2 after 10,000 charge–discharge cycles.

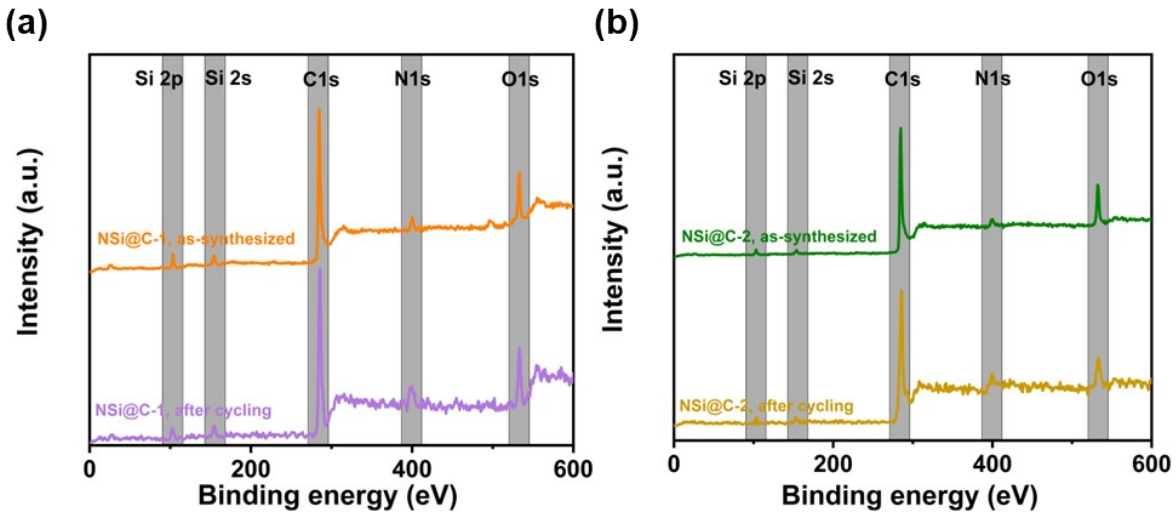

Figure S13. XPS survey spectra of (a) NSi@C-1 and (b) NSi@C-2 as-synthesized and after 10,000 charge–discharge cycles.

Table S7. Comparison Table of the specific capacitance of NSi@C-2 with previously reported redox-active porous polymers.

No	Porous polymers	Capacitance (F g^{-1})	Reff
1	COF/rGO	269, at 0.5 A g^{-1}	[7]
2	BTPP-DBTh	143.27 at 0.5 A g^{-1}	[2]
3	BF-DTDO	95.62, at 0.5 Ag^{-1}	[8]
4	BF-Ph-DTDO	288.8, at 0.5 Ag^{-1}	[8]
5	TAT-CMP-1	141, at 1 A g^{-1}	[9]
6	TAT-CMP-2	183, at 1 A g^{-1}	[9]
7	TPA -Py	78, at 1 A g^{-1}	[10]
8	TPA-Bz	55.1, at 1 A g^{-1}	[10]
9	BT-PDI	196, at 1 A g^{-1}	[11]
10	c-DDSQ-MDA BMI	73.6, at 0.5 A g^{-1}	[12]
11	cNPIMEA TB_80	46, at 1 A g–1	[13]
12	CoPc CMP/CNTs-2	107.2, at 1 A g–1	[14]
13	GH-CMP	182.7, at 0.5 A g^{-1}	[15]
14	CAP-2	233, at 1 A g^{-1}	[16]
15	An-TPP POP	38.12, at 1 A g^{-1}	[17]
16	An-TPA POP	117.7, at 1 A g^{-1}	[17]
17	**NSi@C-1**	**133, at 0.5 A g^{-1}**	**This work**
18	**NSi@C-2**	**403, at 0.5 A g^{-1}**	**This work**

Table S8. Comparison Table of the specific capacitance of NSi@C-2 with previously reported heteroatom-doped carbon materials.

No	Doped carbon materials	Capacitance (F g^{-1})	Reff
1	NPCC-550	191, at 1 A g^{-1}	[18]
2	NPCC-650	200 at 1A g^{-1}	[18]
3	PC-R6A7	366, at 20 A g^{-1}	[19]
4	OPBNP	289 F g^{-1} at 5 A g^{-1}	[20]
5	MCNMs	282, at 0.2 A g^{-1}	[21]
6	NPC-1.5	371, at 1 A g^{-1}	[22]
7	OMC-2	326, at 0.5 A g^{-1}	[23]
8	OSC	354, at 1 A g^{-1}`	[24]
9	S, N-PIC-1	235.3, at 0.5 A g^{-1}	[25]
10	PCNs/GCNs-5	388, at 1 A g^{-1}	[26]
11	N-doped C/rGO	234, at 0.8 A g^{-1}	[27]
12	BC-SA-0.5CP	324.85 at 0.5 A/g	[28]
13	**NSi@C-1**	**133, at 0.5 A g^{-1}**	**This work**
14	**NSi@C-2**	**403, at 0.5 A g^{-1}**	**This work**

S12. Computational Methodology

Density functional theory (DFT) calculations were conducted using Materials Studio software.[29] Representative carbon cluster models of NSi@C-1, NSi@C-2, and a Si-free control (N@C-2) were constructed to reflect the experimentally identified heteroatom environments and optimized with DMol3. Electrolyte adsorption in aqueous KOH was screened using the Adsorption Locator module, with explicit water (100 H2O) and KOH introduced as ionic species (K^+/OH^-), employing Monte Carlo sampling to find stable adsorption configurations. Adsorption affinities were assessed using the adsorption energies (Eads) and the deformation energy (Edef). The electrostatic potential (ESP) and density of states (DOS) were calculated on the optimized structures to compare interfacial polarity and frontier electronic accessibility.

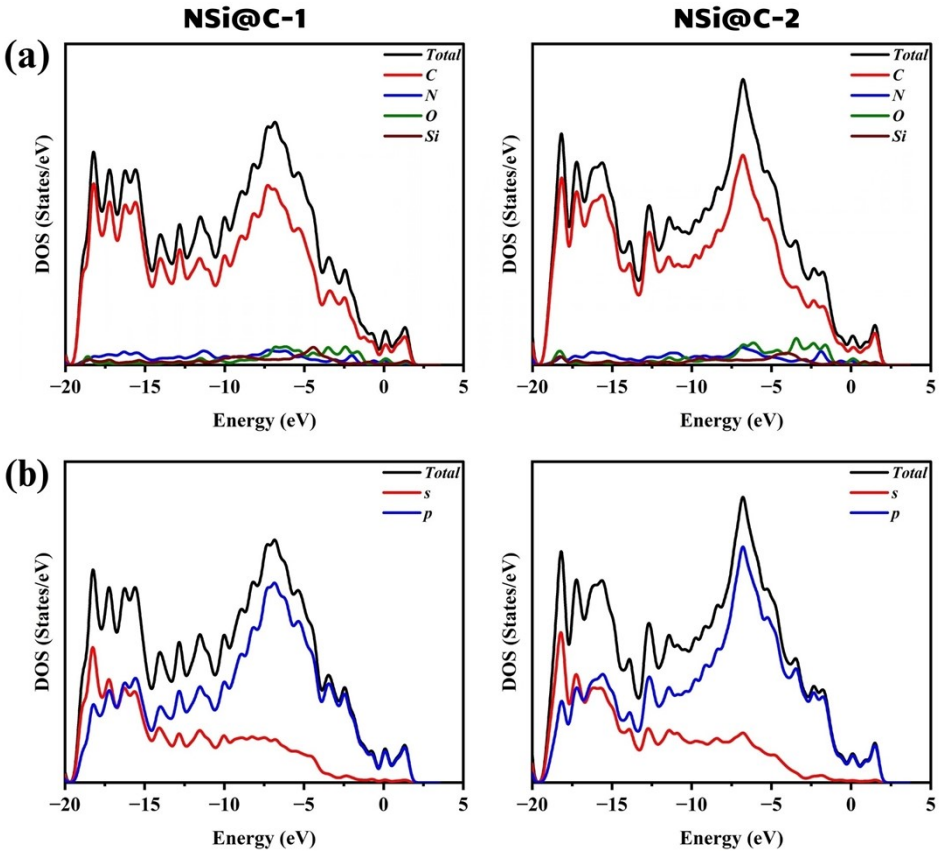

Figure S14. Density of states (DOS) for NSi@C-1 and NSi@C-2. (a) Element-projected DOS, and (b) Orbital-projected DOS.

Table S9. MC simulation results for adsorption of KOH (aq) on the optimized carbon clusters.

Structure	E_{ads} (kcal/mol)	E_{def} (kcal/mol)	K: dE_{ad}/dNi (kcal/mol)	H_2O: E_{ad}/dNi (kcal/mol)
N@C-2 (Si-free model)	-282.05	0.211	-0.548	-2.05
NSi@C-1	-284.12	0.257	-0.599	-1.76
NSi@C-2	-289.10	0.035	-0.777	-2.04

S13. Electrochemical Analysis in Two-Electrode Symmetric Supercapacitor System.

The electrode slurry was composed of SiN@C (70 wt%), carbon black (20 wt%), and Nafion (10 wt%). The mixture was uniformly applied onto a Kuraray carbon paper substrate (thickness: 0.10 ± 0.01 mm) with an active area of 1 cm × 1 cm, followed by drying at 100 °C overnight in a vacuum oven. The total mass loading of active material on the current collector was maintained at 0.79 mg cm^{-2}. A filter paper saturated with 3 M aqueous KOH solution was used as the separator between the two identical electrodes.

The specific capacitance (C_s, F g^{-1}) was determined from galvanostatic charge–discharge (GCD) measurements according to Equation (S4):[2]

$$C_s = \frac{2I\Delta t}{m\Delta V} \qquad \text{(S4)}$$

where I (A) is the discharge current, Δt (s) represents the discharge time, ΔV (V) is the potential window, and m (g) denotes the mass of conjugated polymer on a single electrode. The factor of 2 accounts for the series configuration of the symmetric supercapacitor cell.

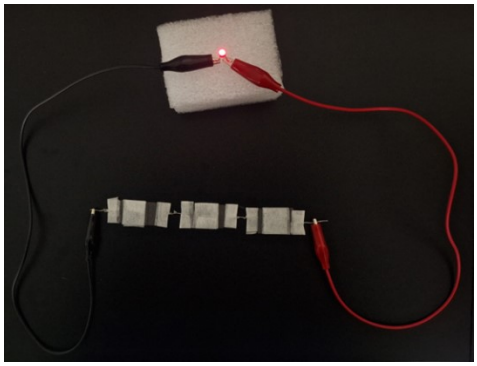

Figure S15. Three NSi@C-2-based SSC devices connected in series successfully powered a red LED.

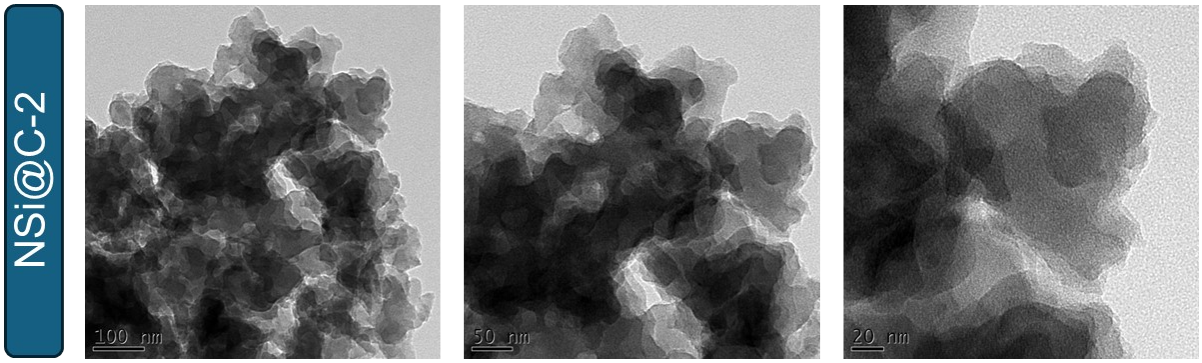

Figure S16. TEM images of NSi@C-2-based symmetric supercapacitor device after 10,000 charge–discharge cycles.

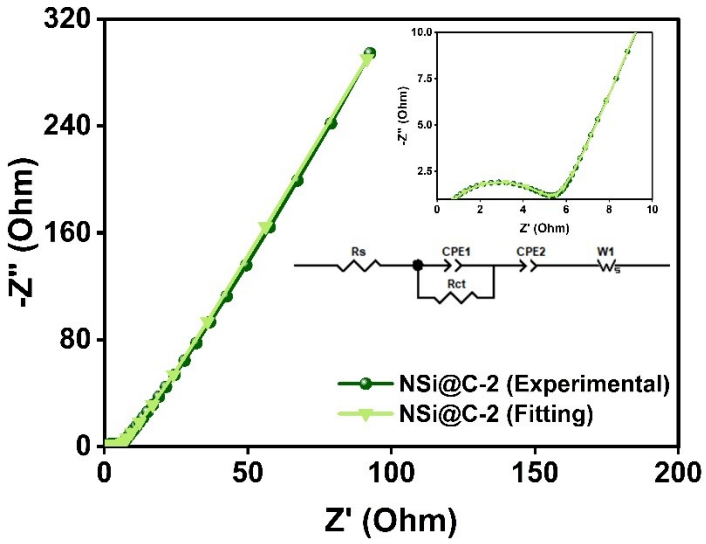

Figure S17. Nyquist plots and corresponding fitting curves of NSi@C-2-based symmetric supercapacitor device.

Table S10. Comparison table of the specific capacitance of NSi@C-2-based device with previously reported porous redox-active polymers and heteroatom-doped carbon materials.

No	Electrode materials	Capacitance (F g^{-1})	Reff
1	SNACM-2	142, at 1 A g^{-1}	[30]
2	BNC-180 SC	43.0, at 0.5 A g^{-1}	[31]
3	NP-AC	45.8, at 0.5 A g^{-1}	[32]
4	SP2 polymer	33.6, at 2 A g^{-1}	[33]
5	LE-P-2||P-2	85.4, at 0.25 A g^{-1}	[34]
6	QSS-P-2||P-2	84.2, at 0.25 A g^{-1}	[34]
7	TBDT-DPP	36, at 1 A g^{-1}	[35]
8	AC-PVA/PVP/Co-1	88, at 0.5 A g^{-1}	[36]
9	PSC-3	37, at 0.5 A g^{-1}	[37]
10	BC-PT CMP	107, at 1.2 A g^{-1}	[38]
11	AC in 1M Na2SO4	94, at 0.2 A g^{-1}	[39]
12	**NSi@C-2**	**211, at 0.2 A g^{-1}**	**This work**

S14. References.

1. L. Liang, J. T. Wang, C. Y. Mei and W.S. Li, *Polymer*, 2013, **54**, 2278-2284.
2. S. Abdelnaser, S. W. Kuo and A. F. M. EL-Mahdy, J. Power Sources., 2025, 635, 236535
3. A. F. M. EL-Mahdy, C. Young, J. Kim, J. You, Y. Yamauchi and S. W. Kuo, *ACS Appl. Mater. Interfaces*, 2019, **11**, 9343-9354.

4. C. R. DeBlase, K. E. Silberstein, T. T. Truong, H. D. Abruña and W. R. Dichtel, *J. Am. Chem. Soc.*, 2013, **135**, 16821-16824.
5. J. Zhan and A. F. M. EL-Mahdy, *Chem. Eng. J.*, 2023, **473**, 145124.
6. A. Alabadi, X. Yang, Z. Dong, Z. Li and B. Tan, *J. Mater. Chem. A.*, 2014, **2**, 11697-11705.
7. C. Li, J. Yang, P. Pachfule, S. Li, M. Y. Ye, J. Schmidt and A. Thomas, Nat. Commun., 2020, 11, 4712.
8. S. X. Liao and A. F. M. EL-Mahdy, *ACS Appl. Energy Mater.*, 2025, **8**, 3074-3086.
9. X. C. Li, Y. Zhang, C. Y. Wang, Y. Wan, W. Y. Lai, H. Pang and W. Huang, Chem. Sci., 2017, 8, 2959-2965.
10. M. G. Kotp, S. U. Sharma, J. T. Lee, A. F. M. EL-Mahdy and S. W. Kuo, J. Taiwan Inst. Chem. Eng., 2022, 134, 104310.
11. S. K. Pati, D. Patra, S. Muduli, S. Mishra and S. Park, J. Mater. Chem. A., 2024, 12, 21165-21175.
12. Z. Y. Chen, W. C. Chen and S. W. Kuo, Polym. Chem., 2024, 15, 553-564.
13. J. W. Jeon, J. Shin, J. Lee, J. H. Baik, R. Malpass-Evans, N. B. McKeown, T. H. Kim, J. C. Lee, S. (S24) K. Kim and B. G. Kim, Appl. Surf. Sci., 2020, 530, 147146.
14. L. Mei, X. Cui, Q. Duan, Y. Li, X. Lv and H. g. Wang, Int. J. Hydrogen Energy., 2020, 45, 22950 22958.
15. M. Zhang, T. Zhao, J. Dou, Z. Xu, W. Zhang, X. Chen, X. Wang and B. Zhou, ChemElectroChem, 2019, 6, 5946-5950.
16. W. Liu, M. Ulaganathan, I. Abdelwahab, X. Luo, Z. Chen, S. J. R. Tan, X. Wang, Y. Liu, D. Geng, Y. Bao, J. Chen, and k. P. Loh, ACS Nano, 2018, 12, 852-860.
17. A. F. Saber, S. Abdelnaser, A. F. M. EL-Mahdy and S. W. Kuo, Electrochim. Acta., 2025, 511, 145397.

18. L. Zhang, X. Li, L. Li, X. Cheng, H. Wu and J. Zheng, *J. Energy Storage*, 2024, **96**, 112680.

19. Y. Li, Y. Zhang, Q. Zhang, X. Shen, Y. Li, J. Wang, R. Gao and R. Li, *J. Energy Storage*, 2024, **102**, 114065.

20. Y. Li, X. Zou, S. Li, Y. Chen, G. Wang, H. Yang and H. Tian, *J. Mater. Chem. A.*, 2024, **12**, 18324-18337.

21. C. Ma, G. Song, Z. Li, H. Wu, C. Wang, Y. Wang, X. Zhang, Y. Song and J. Shi, *J. Energy Storage*, 2024, **88**, 111465.

22. A. Liu, L. Yan, Y. Zhang, R. Ma, N. Guo, L. Wang, B. Zhang, D. Jia and R. Sheng, *Surfaces and Interfaces*, 2024, **44**, 103754.

23. R. Zhang, H. Liu, Z. Cui, Y. Zhang and Y. Wang, *Fuel*, 2024, **364**, 131062.

24. H. Li, T. Du, Q. Wang, J. Guo, S. Zhang and Y. Lu, *J. Energy Storage*, 2023, **66**, 107397.

25. S. Wu, X. Yan, X. Sun, S. Tian, J. Wang, C. Liu, S. Sun, L. Wu, X. Zhao and Q. Yang, *J. Energy Storage*, 2023, **71**, 108152.

26. G. Zhang, Y. Zhang, J. Wang, J. Yu, K. Wang, G. Li and T. Guan, *J. Colloid Interface Sci.*, 2024, **660**, 478-489.

27. S. A. Al Kiey and H. N. Abdelhamid, *J. Energy Storage*, 2022, **55**, 105449.

28. W. Yue, Z. Yu, X. Zhang, H. Liu, Y. Zhang and X. Ma, *J. Anal. Appl. Pyrolysis*, 2024, **179**, 106525.

29. Dassault Systems Materials Studio, BIOVIA, 5005 Wateridge Vista Drive, San Diego, CA 92121, USA, (2017).

30. S. C. Abbas, Z. Hua, Q. Deng, M. S. Ahommed, J. Guo, H. Huang, X. Ma, S. Cao, H. Huang, X. Ma, S. Cao and Y. Ni, *EcoMat.*, 2024, **6**, e12434.

31. L. Luo, J. Deng, Q. Zhang, Y. Lan, G. Du, M. Fan and W. Zhao, *J. Alloys Compd.*, 2025, **1010**, 177094.

32. J. Zheng, T. Cao, B. Ding, X. Zhang, H. Wu and X. Li, *J. Energy Storage*, 2025, **110**, 115297.

33. D. Patra, S. K. Pati and S. Park, *Eur. Polym. J.*, 2024, **212**, 113055.

34. A. A. Wavhal, S. Dilwale, P. P. Puthiyaveetil, N. R. Kakde, M. Prakash, S. Kurungot and S. K. Asha, *J. Phys. Chem. C*, 2024, **128**, 12808-12821.

35. D. Patra, S. K. Pati, S. Muduli, S. Mishra and S. Park, *J. Chem. Eng.*, 2024, **482**, 149162.

36. D. T. Bakhoum, S. Sarr, V. M. Maphiri, N. F. Sylla, N. M. Ndiaye, M. Diop, B. D. Ngom, M. Chaker and N. Manyala, *J. Energy Storage*, 2024, **80**, 110353.

37. X. Cheng, L. Zhang, L. Li, X. Li, H. Wu, J. Zheng, J. Yao and G. Li, *Colloids Surf A Physicochem Eng Asp*, 2024, **698**, 134542.

38. A. F. Saber, Y. F. Chen, L. Mabuti, S. V. Chaganti, S. U. Sharma, J. Lüder, J. T. Lee, S. W. Kuo and A. F. M. EL-Mahdy, *Mater. Adv.*, 2025, **6**, 607-616.

39. K. Gajewska, A. Moyseowicz, D. Minta and G. Gryglewicz, *J Mater Sci*, 2023, **58**, 1721-1738.